Bandpass engineering of lithographically scribed channel-waveguide Bragg gratings

Christoph Greiner, Thomas W. Mossberg, and Dmitri Iazikov

LightSmyth Technologies, Inc., Suite 250, 860 West Park Street, Eugene, Oregon 97041

Received October 20, 2003

We propose and demonstrate a powerful approach to spectral bandpass engineering (apodization) of one-dimensional channel-waveguide Bragg reflectors. Bandpass engineering is accomplished by precise photolithographic control of the length and the longitudinal placement of individual grating lines, which provides unique line-by-line diffractive amplitude and phase control. Channel-waveguide gratings that exhibit complex filtering functions have been fabricated and modeled. When a second-order apodization effect that comprises effective waveguide refractive-index variation with grating-line length is included in the simulation, extraordinary agreement between predicted and observed spectral passband profiles is obtained. © 2004 Optical Society of America

OCIS codes: 130.3120, 050.7330, 060.2310, 050.1950.

An inherent strength of Bragg reflectors is that, in principle, they can be designed to implement a broad range of spectral filtering and processing functions. For weakly reflecting devices, the grating's reflection spectrum is simply related to the spatial Fourier transform of the effective reflection coefficient expressed as a function of position into the grating. It follows that the key to engineering of virtually arbitrary spectral filtering and processing functions is the ability to precisely control reflective amplitude and phase as a function of depth into the grating—preferably on an individual grating-line basis. We introduce here an approach to achieving such control and demonstrate through device fabrication the complex spectral filtering functions that it enables.

One-dimensional Bragg structures may be created in fibers or in channel waveguides by use of surface relief[1,2] or volumetric[3] diffractive surfaces and may be apodized in various ways.[4–13] Apodization methods demonstrated previously do not provide for sufficiently high-resolution (line-by-line) control of diffractive element (grating-line) amplitude and phase. Recently we demonstrated[14] that photolithographic writing of slab-waveguide-based two-dimensional Bragg structures provides control of the reflective amplitude and phase of grating-constituent diffractive elements on a truly line-by-line basis. Here we demonstrate a different apodization approach that is useful for one-dimensional lithographically scribed Bragg gratings contained in channel waveguides. The method is based on controlling the reflective amplitude of individual grating lines by adjustment of their length (transverse to the channel waveguide). Phase control of light reflected from each grating line is achieved by means of spatial displacement along the waveguide axis. The present channel-waveguide grating apodization method is, to our knowledge, unprecedented in its ability to manipulate reflective amplitude and phase of individual grating lines. Line-by-line controllability stems from the apodization scheme and its method of implementation, i.e., by computer design, laser-written photomask, and deep-UV photolithographic fabrication.

Figure 1(a) is a cross-sectional side view of the silica-on-silicon channel-waveguide Bragg grating. Grating lines, shown as filled rectangles, are located at the interface between waveguide core and upper cladding and are oriented perpendicular to the figure's plane. The waveguide has a rectangular, 6.4 μm (width w) $\times$ 2 μm (height h), central core. The core's index contrast relative to the surrounding cladding layers (with $\geq$15-μm thickness) is +0.8%. The grating's diffractive elements (lines) are trenches with depth $d \approx 400$ nm that we created by etching into the core and subsequently filling it with cladding material. The grating operates in first diffraction order with a period Λ of $\sim$500 nm.

Figure 1(b) is a top view of an exemplary channel waveguide grating apodized by the present method by use of a sinc function. The optical signal enters the filter from the left side. The resonant input beam interacts with the diffractive elements of the Bragg grating (lines) and is coherently backscattered antiparallel to the input. In Fig. 1(b) the net reflected field $E_r{}^k(\mathbf{r})$ from an individual grating line k is proportional to the integral of the product of input field $E_{\text{in}}(\mathbf{r})$ and line

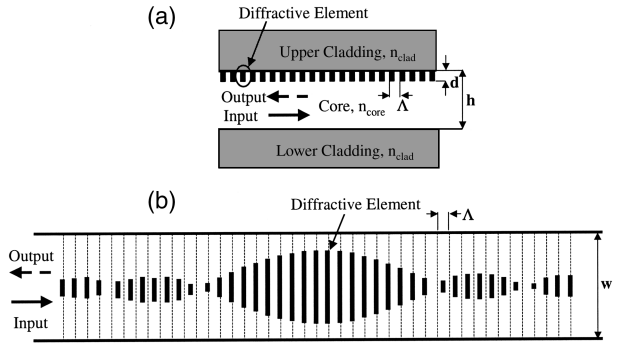


Fig. 1. (a) Schematic cross-sectional view (the cut plane is perpendicular to the grating lines) of a channel-waveguide Bragg reflector. (b) Schematic top view (looking down on the grating trenches). d, grating depth; h (w), waveguide core height (width); Λ, grating period. The apodization function shown is exemplary and differs from those implemented in fabricated devices.

0146-9592/04/080806-03$15.00/0 © 2004 Optical Society of America

reflection coefficient $r_k(\mathbf{r})$ evaluated along the line's length, i.e.,

$$E_r{}^k \propto \int_{\text{line } k} E_{\text{in}}(\mathbf{r}) r_k(\mathbf{r}) \mathrm{d}\mathbf{r}\,. \tag{1}$$

Amplitude apodization may be achieved through control of grating-line reflection coefficient $r_k(\mathbf{r})$ by, for example, control of trench depth d, of the length of the line, or both. Because the process of lithographic fabrication strongly favors a uniform etch depth, amplitude apodization by control of grating-line length as demonstrated here is highly advantageous.

In the research reported here, continuous amplitude apodization functions were approximated by a 42-level scale with each amplitude level corresponding to a specific line length. The grating-line lengths employed spanned the range 0–4.1 μm, with discrete values separated by 100-nm increments. When the transverse dependence of the input field mode distribution is taken into account, the relationship between reflected field amplitude and grating-line length becomes nonlinear. For translation of the apodization amplitude into line length, a model input field with Gaussian transverse distribution ($1/e$ half-width of 3.35 μm) was assumed. As shown in Fig. 1(b), one achieves control of grating-line reflective phase by displacing the grating line by an appropriate spatial offset from the nominally equal grating-period position (shown in the figure as dashed thin lines). In this manner, arbitrarily reflected field phase shifts can be achieved, with a $\pm\pi$ phase shift corresponding to a $\pm\Lambda/2$ displacement to the left (+) or right (−).

To demonstrate the power and flexibility of this apodization approach, we designed and fabricated two channel-waveguide filters with quite different spectral transfer functions. The simulated and achieved spectral responses of these devices are displayed in Fig. 2. A first channel-waveguide Bragg filter was designed to have a 4-nm-wide flat-top spectral passband. The grating had a length of ~1.1 cm. The grating pitch was chirped to create the 4-nm bandwidth. An additional phase and super-Gaussian amplitude apodization were employed to minimize passband ripple.

Figure 2(a) depicts the first passband profile calculated from the computer-generated spatial design by a Fresnel–Huygens diffraction method. Figure 2(b) gives the measured spectral transfer function of the fabricated device for TE-polarized input light. The achieved passband profile closely reproduces the designed passband. The measured insertion loss (IL) was ~8 dB, which includes ~1 dB for fiber-to-waveguide coupling. The slight passband ripple at the filter's short-wavelength side and the slower (compared with that of the design) long-wavelength falloff arise from a second-order apodization effect that comprises an effective refractive-index variation concomitant with amplitude apodization. Measurements of various test grating structures, each with grating lines of fixed length, showed a small and approximately linear variation of effective waveguide refractive index with grating-line length. The fractional effective index difference between a waveguide without a grating and one with a grating whose lines are of maximal line length was found to be -2×10^{-4}. Figure 2(c) shows the simulated passband profile with inclusion of the measured apodization-induced effective refractive-index change. The simulation now clearly reproduces all features of the fabricated device.

As a second example of spectral passband engineering by the present apodization method, we designed a multipeak spectral filter. The 19-mm-long grating has eight, approximately 1-nm-wide, spectral peaks spanning a total bandwidth of 15 nm. To span such a large spectral region, the grating period Λ is stepped and chirped. Tailored phase modulation is introduced to reduce spectral ripples. Figure 2(d) is a Fresnel–Huygens diffraction calculation of the bandpass function expected from the computer-generated design. Figure 2(e) shows the measured relative reflection spectrum for TE input polarization. The insertion loss observed, including fiber coupling, was ~8.5 dB, implying an intrinsic device IL of ~7.5 dB. Although the measured bandpass profile of Fig. 2(e) is in general agreement with the constant-index calculation of Fig. 2(d), some distortions are evident. In Fig. 2(f) a bandpass simulation based on fabricated grating design and incorporating the effective

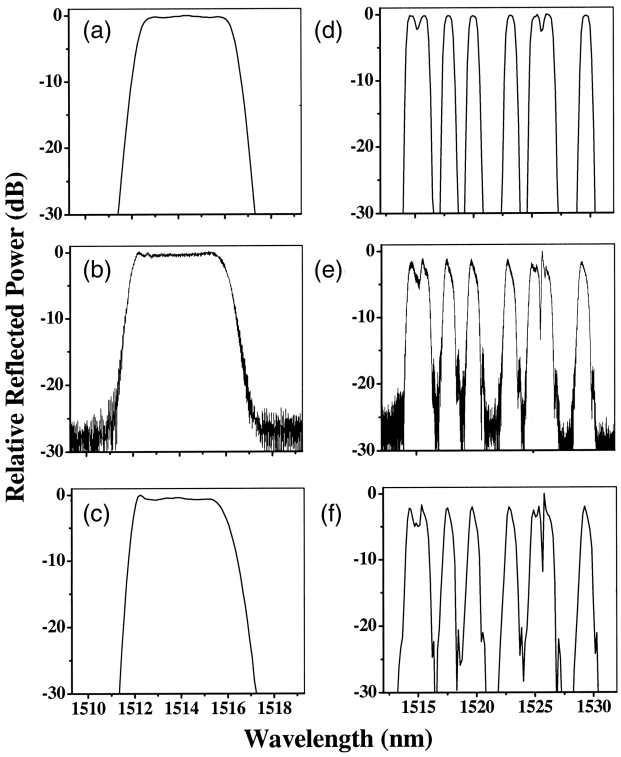


Fig. 2. (a) Simulated flat-top filter with constant-waveguide effective refractive index, (b) measured channel-waveguide reflection spectrum, (c) simulated flat-top filter with apodization-dependent effective refractive index, (d) simulated multicolor filter with constant refractive index, (e) measured channel-waveguide reflection spectrum, (f) simulated multicolor filter with apodization-dependent effective refractive index. In each figure the peak reflected power is normalized to 0 dB.

index dependence on amplitude apodization is given. The agreement between Fig. 2(f) and the measured bandpass spectrum of Fig. 2(e) is remarkable. We conclude that design algorithms that incorporate the observed coupling between effective index and amplitude apodization will produce passbands that are precisely as designed.

When the multipeak spectral filter is measured in transmission at the wavelength of peak reflected power, an IL of 0.81 (±0.05) dB is observed. This measured transmission loss is consistent with the 7.44- (±0.19-) dB IL measured in reflection. Both of those measurements exclude fiber-to-waveguide coupling loss. Since, within measurement accuracy, reflected and transmitted power add to unity, we conclude that losses due to absorption or to coupling to cladding modes are not significant. Increases in index contrast and trench depth are projected to enable devices with 1–2-dB reflective IL and bandwidths in excess of 100 nm.

The measurements shown in this Letter employed TE-polarized input signals. For TM input the grating bandpass functions were observed to shift by approximately +0.15 nm and to exhibit an additional insertion loss of 1.2 (±0.1) dB, which can be decomposed into a grating-intrinsic polarization-dependent loss of 0.8 (±0.2) dB and a channel-waveguide–fiber coupling polarization-dependent loss of 0.4 (±0.1) dB. Changes in reflective bandwidth with polarization indicate that observed grating-intrinsic polarization-dependent loss stems from a polarization-dependent grating reflectivity rather than from power loss. Measurements of first- and fourth-order unapodized reference gratings collocated in a single-channel waveguide reveal polarization-dependent wavelength shifts of 0.18 and 0.15 nm, respectively. As grating-mediated wavelength shifts should be roughly four times smaller in the higher-order grating, we conclude that the polarization-mediated wavelength shift observed stems primarily from waveguide birefringence.

The observed polarization-dependent wavelength shift indicates an aggregate (fractional) birefringence of magnitude 1×10^{-4}. A simulation based on the beam propagation method found the form birefringence for a 2 μm × 6 μm waveguide to be only 2×10^{-5}. This result suggests that the observed birefringence is largely attributable to strain, a known problem of the silica-on-silicon platform that may be overcome by use of strain-relieving grooves yielding essentially polarization-independent gratings.[15] We furthermore note that the subnanometer wavelength shifts observed here do not interfere with proper operation of wide-passband devices such as the one demonstrated in Figs. 2(a)–2(c).

In summary, we have proposed and demonstrated a novel apodization concept for lithographically scribed one-dimensional Bragg gratings that, together with computer-generated design, laser photomask writing, and deep-UV reduction lithography, provides complete control of amplitude and phase of individual grating lines. We have demonstrated its application to several devices with tailored spectral transfer functions. An amplitude-apodization-dependent variation in effective waveguide refractive index has been identified whose inclusion in design algorithms promises the production of highly accurate spectral profiles.

C. Greiner's e-mail address is cgreiner@lightsmyth.com.

References

1. C. M. Ragdale, D. Reid, D. J. Robbins, J. Buus, and I. Bennion, J. Sel. Areas Commun. **8,** 1146 (1990).
2. M. Horita, S. Tanaka, and Y. Matsushima, Electron. Lett. **34,** 2240 (1998).
3. R. Kashyap, *Fiber Bragg Gratings* (Academic, San Diego, Calif., 1999).
4. T. Erdogan, J. Lightwave Technol. **15,** 1277 (1997).
5. J. L. Rebola and A. V. T. Cartaxo, J. Lightwave Technol. **8,** 1537 (2002).
6. A. Carballar, M. A. Muriel, and J. Azana, IEEE Photon. Technol. Lett. **11,** 694 (1999).
7. T. Komukai, K. Tamura, and M. Nakazawa, IEEE Photon. Technol. Lett. **9,** 934 (1997).
8. C. Marra, A. Nirmalathas, D. Novak, C. Lim, L. Reekie, J. A. Besley, C. Weeks, and N. Baker, J. Lightwave Technol. **21,** 32 (2003).
9. K. O. Hill, B. Malo, F. Bilodeau, S. Theriault, D. C. Johnson, and J. Albert, Opt. Lett. **20,** 1438 (1995).
10. A. Grunnet-Jepsen, A. E. Johnson, E. S. Maniloff, T. W. Mossberg, M. J. Munroe, and J. N. Sweetser, Electron. Lett. **35,** 1096 (1999).
11. D. Wiesmann, C. David, R. Germann, D. Erni, and G. L. Bona, IEEE Photon. Technol. Lett. **12,** 639 (2000).
12. D. Wiesmann, R. Germann, G. L. Bona, C. David, D. Erni, and H. Jackel, J. Opt. Soc. Am. B **20,** 417 (2003).
13. Y. Shibata, T. Tamamura, S. Oku, and Y. Kondo, IEEE Photon. Technol. Lett. **6,** 1222 (1994).
14. C. Greiner, D. Iazikov, and T. W. Mossberg, "Lithography fabricated planar holographic Bragg reflectors," J. Lightwave Technol. (to be published).
15. R. Adar, C. H. Henry, R. H. Kistler, and R. F. Kazarinov, Appl. Phys. Lett. **60,** 1779 (1992).

Copyright OSA. This paper was published in Optics Letters and is made available as an electronic reprint with the permission of OSA. One copy may be made for personal use only. Systematic or multiple reproduction or distribution to multiple locations via electronic or other means, duplication of any material in this paper for a fee or for commercial purposes, or modificaiton of the content of the paper are prohibited (www.osa.org/pubs/osajournals.org).